Available online at www.sciencedirect.com
ScienceDirect
Trans. Nonferrous Met. Soc. China 24(2014) 2695−2703
Transactions of Nonferrous Metals Society of China
www.tnmsc.cn

Noisy-power dissipation and efficiency in NiO/Fe_2O_3 wet grinding by planetary ball mill

Yun YAO[1], Gang XIE[1,2], Yan-qing HOU[1], Rong-xing LI[1], Wei-hong LUO[1], Ru-zhen PENG[1], Zhan-liang YU[2]

1. Faculty of Metallurgical and Energy Engineering, Kunming University of Science and Technology, Kunming 650093, China;
2. Kunming Metallurgy Research Institution, Kunming 650031, China

Received 20 May 2013; accepted 14 April 2014

Abstract: The relationship between the efficiency of NiO/Fe_2O_3 wet grinding and noisy-power dissipation was studied. The optimal grinding parameters were found as: a slurry water content of 64.10%−85.47%, ball number ratio of 360/20, revolution speed of 300.9 r/min, powder-filling ratio of 10.88%, ball-filling ratio of 20.53%−23.88%, and grinding time of approximately 6 h. The discrete element method (DEM) was employed to analyze relationship between the noisy-power dissipation and the grinding efficiency, and equations describing the relationship were derived. The mean particle size of the ground powder decreased with a decrease in the degree of noisy-power dissipation, while the grinding efficiency and the amount of specific impact power used decreased with an increase in the degree of noisy-power dissipation.

Key words: noisy-power dissipation; NiO/Fe_2O_3 powder; planetary ball mill; mean particle size

1 Introduction

Interest in alloy and cermet materials for fabricating inert anodes for use in industrial aluminum electrolysis has increased in recent years because of their significant advantages in terms of energy, cost, productivity, and environmental benefits [1−8]. $NiFe_2O_4$-based cermet is one of the most promising materials studied in recent years, due to its high electrical conductivity and corrosion resistance [6,9]. However, the performance of the inert anode fabricated from $NiFe_2O_4$-based cermet could not satisfy the requirements for aluminum electrolysis because of unsuitable mechanical properties and insufficient corrosion resistance and electrical conductivity.

Generally, ball milling and sintering techniques have been used to produce $NiFe_2O_4$-based cermet. However, well-blended, fine granular NiO/Fe_2O_3, which is the precursor of $NiFe_2O_4$, must be prepared first. The planetary ball mill is one of the most popular equipments for grinding NiO/Fe_2O_3 because of its moderate cost and simple setup and handling [7,10,11]. Researchers identified that the grinding efficiency of planetary ball mill depends on several factors, such as pot diameter, pot depth, ball diameter, ball-filling ratio, revolution radius, material-filling ratio, and rotational speed [12,13]. Further, the impact energy between balls and powders, frequency of impacts, and abrasion are major factors that influence the working of planetary ball mills, and these factors are related to the ball–ball, ball–container, ball–powder, and powder–powder impact energy and collision frequency [14,15]. The specific impact energy is a useful parameter for analyzing the grinding mechanism and granular media performance [12−14,16]. However, few systematic experimental investigations conducted to date have focused on technical parameters, noisy-power dissipation, and efficiency in NiO/Fe_2O_3 grinding because observing the motion of the balls within the mills and evaluating the performance of the mills are difficult. In fact, studies on NiO/Fe_2O_3 grinding and their noisy-power dissipation are seldom reported nowadays.

In recent years, the discrete element method (DEM) [10,14,15,17−19], particle element method (PEM) [20], and modified version of the distinct element method (MDEM) [21] have been utilized to investigate specific impact energy dissipation in the case of materials such as

Corresponding author: Yun YAO; Tel: +86-13529373085; E-mail: yyaoun1982@aliyun.com
DOI: 10.1016/S1003-6326(14)63400-2

gibbsite [13,14,22], limestone [22], and talc [16]. In particular, the DEM is one of the most powerful techniques for investigating the granular-media grinding mechanism and performance.

Therefore, in this study, the DEM is employed to analyze the water-filling ratio, number ratio of balls with diameters of 10 mm and 20 mm, revolution speed, powder-filling ratio, ball-filling ratio, grinding time, and the relationship between grinding efficiency and noisy-power dissipation in the grinding of NiO/Fe_2O_3. Three major mechanical energy dissipation modes were found during planetary ball milling operation: efficient energy absorption by the ground powder, noisy-power dissipation, and thermal energy generation as a result of heating of the granular media, pots, and gas during grinding. The efficient energy absorbed by ground powder and noisy-power dissipation should not be omitted in the balls motion, but thermal energy of heating granular media grinding, pots and gas is very small because the temperature is homogeneous during the grinding.

2 Experimental

2.1 Equipment and chemical reagents

The grinding mill used in this study was a planetary ball mill (XQM-4L, China). The mill consisted of four pots made of stainless steel (density, ρ=8.2×10^3 kg/m^3) placed on a revolving disk. The volume, inner diameter, and height of the pots were 1l, 118, and 92 mm, respectively. The grinding media were dual-sized balls (diameters of 10 mm, 20 mm) made of stainless steel. The rotational speed, r, which was determined by the rotation-to-revolution speed ratio of the planetary ball mill, was set to be 1.00 for the study (r=N_P/N_r, where N_P is the rotation speed of the pots and N_r is the revolution speed of the disk). The revolution speed of the disk could be varied from 50 to 400 r/min, and the rotation speed of the disk could be varied from 100 to 800 r/min. The planetary ball mill was set to alternately rotate and revolve in the clockwise and anticlockwise directions at intervals of 5 min. The pot was set to rotate counter to the direction of revolution of the disk.

The acoustic test instrument employed in the study was an AR824 digital sound level meter (Smart Sensor, China) and was used to test the level of noisy-power dissipation in the planetary ball mill. During the working of the ball mill, the output of the digital meter increased with an increase in the amount of power dissipated. Thus, the digital sound level meter could evaluate the efficiency of grinding indirectly.

The sizes of the particles of the samples to be ground were measured using the sedimentation method. Ethanol (CH_3CH_2OH; minimum concentration of 99.8%) was employed as the liquid for the measurements. The sedimentation method for determining the particle size is based on the fact that particles were smaller in size when displace in larger volume of suspension (V_s) of ethanol absolute at any point of time. The specific surface areas of the ground powers were characterized by a Nova Win surface area analyzer (Quantachrome Instruments, USA).

The test samples to be ground were a ferric oxide (Fe_2O_3) powder (minimum concentration of 95.76%; Liuzhou Yuejin Chemical Industry Limited Company, China) and a nickel protoxide (NiO) powder (minimum concentration of 99%, Chengdu Nickel Powder Materials LLC, China). The initial diameters of the Fe_2O_3 and NiO powder particles were 47 and 75 μm, respectively. The two powders were mixed in a Fe_2O_3/NiO mass ratio of 57.9/42.1. The Fe_2O_3/NiO mixture was then dispersed in water in different concentrations, and the resulting slurries were used as the starting samples. These samples were placed in each pot of the planetary ball mill and ground. The blended slurries were dried in an oven at 100 °C for 24 h. The blended powders obtained after drying the slurries were dispersed using an agate mortar. As mentioned previously, the particle sizes of the blended powders were measured using the sedimentation method, and their specific surface areas were measured using a surface area analyzer.

2.2 Single-factor experiments

2.2.1 Effect of water content of slurry

200 small balls (diameter of 10 mm) and 40 big balls (diameter of 20 mm) were placed in each stainless steel pot along with 234 g of the powder mixture to be ground. The grinding time and rotation speed were set to be 4 h and 299.5 r/min, respectively. The amount of water added to each pot ranged from 50 g to 450 g. That is to say, the water content of the NiO/Fe_2O_3 slurries was 21.4%−192.3%.

2.2.2 Effect of number ratio of big to small balls

The small (diameter of 10 mm) and big (diameter of 20 mm) steel balls were placed at different number ratios in the stainless steel pots. However, the total volume of the balls was kept constant at ~272.3 cm^3. The numbers of small and big balls used are listed in Table 1. At every stage of the experiment, each pot contained the same number of balls. 234 g of the dry powder was placed in each pot. The grinding time and rotation speed were set to be 4 h and 299.5 r/min, respectively. The amount of water added to each pot was 150 g. That is to say, the water content of the NiO/Fe_2O_3 slurry in each pot was 64.1%.

Table 1 Number ratio of balls with diameters of 10 mm and 20 mm

No.	Number		Number ratio of balls of different diameters
	Small balls (diameter=10 mm)	Big balls (diameter=20 mm)	
1	40	60	40/60
2	80	55	80/55
3	120	50	120/50
4	160	45	160/45
5	200	40	200/40
6	240	35	240/35
7	280	30	280/30
8	320	25	320/25
9	360	20	360/20
10	400	15	400/15

2.2.3 Effect of rotation speed

360 small balls and 20 big ones were placed in each pot. 234 g of the dry powder mixture was also placed in each pot. The grinding time was set to be 4 h. The amount of water added to each pot was 150 g. That is to say, the water content of the NiO/Fe_2O_3 slurry in each pot was 64.1%. The rotation speed was varied from 260.6 to 460.8 r/min.

2.2.4 Effect of powder-filling ratio

360 small balls and 20 big balls were placed in each pot. The total mass of all the balls was 2151.33 g. The amounts of dry powder added to each pot were 116.79, 234.00, 351.00, 468.00, and 585.30 g for ball/powder mass ratios of 5.44%, 10.88%, 16.32%, 21.75%, and 27.21%, respectively. The grinding time and rotation speed were set to be 4 h and 300.9 r/min, respectively. The amount of water added to each pot was 150 g. That is to say, the water content of the NiO/Fe_2O_3 slurry in each pot was 64.1%.

2.2.5 Effect of ball-filling ratio

Balls were placed in the pots in different ball-filling ratios, J. The ball-filling ratios used are listed in Table 2. The amount of dry powder added to each pot was 234.2 g. The grinding time and rotation speed were set to be 4 h and 300.9 r/min, respectively. The amount of water added to each pot was 150 g. That is to say, the water content of the NiO/Fe_2O_3 slurry in each pot was 64.1%.

2.2.6 Effect of grinding time

360 small balls and 20 big ones (the ball-filling ratio was 27.23%) were placed in each pot. The amount of dry powder added to each pot was 234 g. The grinding time, t, was varied from 2 h to 12 h with the mean grinding time being 2 h. The rotation speed was set to be 300.9 r/min. The amount of water added to each pot was 150 g. That is to say, the water content of the NiO/Fe_2O_3 slurry in each pot was 64.1%.

Table 2 Conditions corresponding to different ball-filling ratios

Sample No.	Number of small ball	Number of big ball	Volume of ball/mL	Volume of mill pot/mL	Ball-filling ratio/%
1	200	0	104.72	1000	10.47
2	232	4	138.30	1000	13.83
3	264	8	171.81	1000	17.18
4	296	12	205.31	1000	20.53
5	328	16	238.82	1000	23.88
6	360	20	272.32	1000	27.23
7	392	24	305.82	1000	30.58

3 Results and discussion

During planetary ball milling operations, mechanical energy is dissipated through three major paths. These are the absorption of energy by the powder to be ground, noisy-power dissipation, and the thermal energy released by the heating of the granular media being ground and the pots and gas used in the grinding process. On the basis of the results of this study, the mechanical energy dissipated could be represented by Eq. (1). In this equation, the last term on the right-hand side is usually very small, as the temperature during the grinding process remains constant.

$$P_W=P_{W,m}+P_{W,n}+P_{W,h} \quad (1)$$

where P_W is the specific impact energy of the planetary ball mill; $P_{W,m}$ is the energy absorbed by the granular media to be ground; $P_{W,n}$ is the energy dissipated owing to noisy-power dissipation; $P_{W,h}$ is the thermal energy released by the heating of the granular media to be ground and the pots and gas used.

3.1 Analysis of V_s and $P_{W,n}$ for different slurry water contents

Figure 1 shows the effects of the slurry water content on V_s and $P_{W,n}$ for the parameters listed in Table 3. It can be seen that V_s and $P_{W,n}$ increase initially with an increase in the slurry water content. The value of V_s peaks at 27 mL when the content is 85.5%; the corresponding value of $P_{W,n}$ is 0.0026 J/s. The value of $P_{W,n}$ reaches the maximum (0.0044 J/s) when the content is 42.7%; the corresponding V_s is 18 mL. Further, both V_s and $P_{W,n}$ decease with further increase in the water content.

The above-described phenomena were analyzed using the DEM. Using the DEM, MORI et al [16] had found that the motion of the balls during wet milling is affected by the drag force, F_D, and the buoyancy of the mill balls.

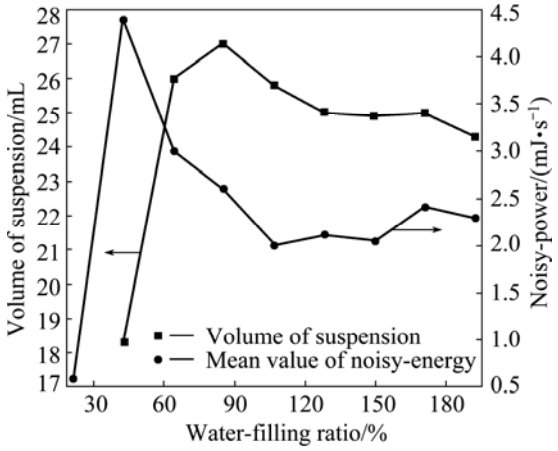

Fig. 1 Relationship among slurry water content, V_s, and $P_{W,n}$

Table 3 Parameters for single-factor experiments

Slurry water content/%	Number ratio of balls	Rotational speed/(r·min^{-1})	Powder amount/g	Ball-filling ratio/%	Grinding time/h
Variable	200/40	299.5	234.0	27.23	4
64.1	Variable	299.5	234.0	27.23	4
64.1	360/20	Variable	234.0	27.23	4
64.1	360/20	300.9	Variable	27.23	4
64.1	360/20	300.9	234.2	Variable	4
64.1	360/20	300.9	234.0	27.23	Variable

The value of F_D can be calculated using Eq. (2). It should be noted that C_d in Eq. (2) is calculated using Eq. (3) and it is a function of the Reynolds number, *Re*, which is given by Eq. (4).

$$F_D = C_d A \rho_s \frac{u_R^2}{2} \tag{2}$$

$$C_d = (0.63 + \frac{4.8}{\sqrt{Re}})^2 \tag{3}$$

$$Re = \frac{d_B |u_R| \rho_s}{\alpha} \tag{4}$$

where C_d is the drag coefficient; A is the projection area of a mall ball; ρ_s is the density of the slurry; u_R is the relative velocity of an individual ball and the slurry; d_B is the diameter of an individual ball; α is the viscosity of the slurry.

According to Eqs. (2)−(4), the phenomenon of grinding shown in Fig. 1 is related to ρ_s, A, u_R, α, and d_B. d_B is assumed to be constant for this experiment. When the water content of the slurry is very small (i.e., the powder mixture in the mill pots is dry), u_R remains constant and *Re* increases with an increase in water content. It should be noted that *Re* is very small since the viscosity of the slurry is high when it is dry, that is, its water content is very low. Therefore, the last term on the right-hand side of Eq. (3) cannot be neglected. Hence, C_d decreases with an increase in *Re*. In addition, F_D decreases with a decrease in C_d, as suggested by Eq. (2). The buoyancy of the balls is also very low when the slurry water content is low. The energy dissipated by the powder is very large because F_D and buoyancy are very small. The first term on the right-hand side of Eq. (1), which results from the force acting on the powder, is very large. Therefore, the value of P_W is determined primarily by the $P_{W,m}$ term, which increases with an increase in V_s.

Secondly, C_d, ρ_s, A, and α decrease and u_R increases with an increase in the slurry water content, that is, as the dry powder becomes a slurry (or as the ground material starts to cover the grinding balls). The grinding process corresponds to a transition state that is affected by both F_D and the buoyancy together. The energy dissipated by the powder is the maximum in this transition state. Therefore, P_W is determined by $P_{W,m}$. Further, V_s is the maximum in this transition state.

In the end, the NiO/Fe_2O_3 powder does not cover the balls completely as the buoyancy of the balls is at the highest value. The value of *Re* is very large, and thus the last term on the right-hand side in Eq. (3) can be neglected. Further, ρ_s, A, u_R, α, d_B, and C_d are constant. Hence, F_D does not vary with an increase in the slurry water content when the water content is very large. Therefore, V_s remains almost constant, and P_W is mostly determined by the $P_{W,n}$ term.

According to Eqs. (2)−(4), V_s decreases (i.e., the particle size is large) when F_D increases. Similarly, V_s increases (i.e., the particle size is small) when F_D decreases. From Fig. 1, it can be seen that V_s reaches the maximum value of 27 mL when $P_{W,n}$ and the water content are 0.003−0.0026 J/s and 64.10%−85.47%, respectively. In this case, the grinding process is the most efficient, and $P_{W,n}$ has the smallest value. Hence, the slurry water content should be controlled to be 64.10%−85.47%. Further, an interesting phenomenon can be seen in Fig. 1, in which the grinding efficiency of the planetary ball mill decreases as the energy dissipated in the form of noisy power increases.

3.2 Analysis of V_s and $P_{W,n}$ for different ball number ratios

Figure 2 shows that V_s and $P_{W,n}$ vary with the number ratio of the balls with diameters of 10 mm and 20 mm as the other parameters listed in Table 3, remain constant. It can be seen from the figure that V_s increases to 40 mL (i.e., the particle size decreases as V_s increases) with an increase in the number ratio; the corresponding $P_{W,n}$ is 0.0023 J/s. Further, V_s decreases with the number

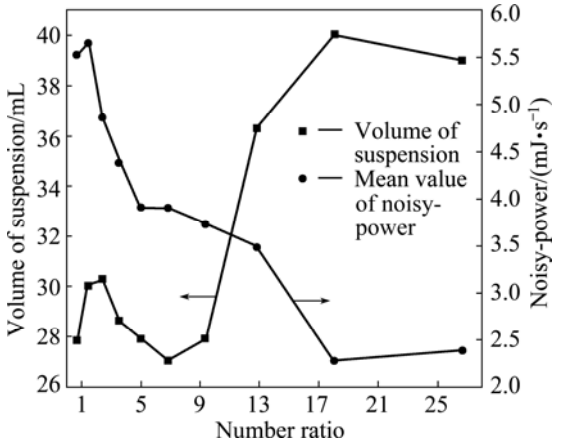

Fig. 2 Relationship among number ratio of balls with diameters of 10 mm and 20 mm, V_s, and $P_{W,n}$

ratio of the balls. However, $P_{W,n}$ increases with an increase in the number ratio.

On the basis of the DEM, ROSENKRANZ et al [10] and MIO et al [12] found that the motion of the mill balls is effective in grinding powders when the motion shifts from cascading-type to cataracting-type during grinding; further, they also noted that the rolling motion of the mill balls was ineffective for grinding. This phenomenon can be interpreted using the Newton's Second Law. For simplicity, considering that a single-mill ball spirals upwards, as shown in Fig. 3. According to the Newton's Second Law, this type of cascading motion can be described by Eq. (5).

$$\mu R\omega^2 \sin\theta \geq g \tag{5}$$

where μ is the friction coefficient; R is the rotation-to-revolution speed ratio; ω is the angular velocity; θ is the angle between the horizontal and vertical directions; g is standard gravity.

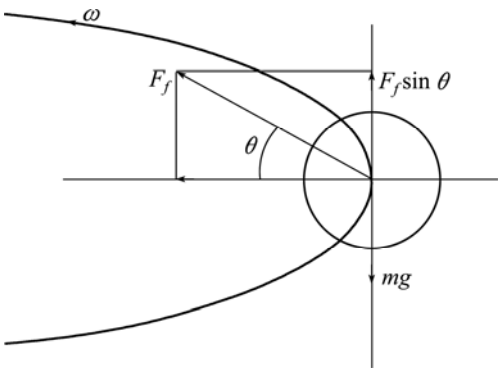

Fig. 3 Force analysis of spiral motion of a mill ball

In Fig. 2 and Eq. (5), R and the rotation and revolution speeds are constants. μ and θ increase with an increase in the number ratio of the balls with diameters of 10 mm and 20 mm. Cascading-type motion takes place when the term on the left-hand side of Eq. (5) is greater than the term on the right-hand side. At this point, the motion shifts from cascading type to cataracting type. The specific impact energy increases when the motion is of the cascading type, suggesting that a greater amount of P_W is absorbed by the NiO/Fe_2O_3 powder, resulting in finer particles. Hence, V_s reaches a high value of 40 mL when the motion is of the cascading type. Subsequently, the motion shifts from the cataracting type to the rolling type when the number ratio is increased further. Rolling-type motion is ineffective for grinding because the rate of collision of the balls decreases considerably and the balls start colliding against the mill walls. Hence, V_s decreases slowly when rolling-type motion occurs.

As can be seen from Fig. 2, $P_{W,n}$ decreases when V_s and the number ratio increase with $P_{W,n}$ exhibiting the lowest value at V_s of 40 mL and number ratio of 360/20. The grinding process is the most efficient when $P_{W,n}$ is the lowest.

3.3 Analysis of V_s and $P_{W,n}$ for different rotation-to-revolution speeds

Figure 4 plots V_s and $P_{W,n}$ as functions of the rotation-to-revolution speed, v; the rest of the parameters were the ones listed in Table 3. Both V_s and $P_{W,n}$ increase with an increase in v. The value of V_s peaks at 40 mL when the rotation-to-revolution speed is 300.9 r/min and $P_{W,n}$ is 2.9 mJ/s. Further, $P_{W,n}$ reaches its maximum value of 7.5 mJ/s when the rotation-to-revolution speed is 420.4 r/min and V_s is 30 mL. Subsequently, both V_s and $P_{W,n}$ decrease for further increases in the rotation-to-revolution speed.

The changes in V_s and $P_{W,n}$ with v can be interpreted on the basis of the value of P_W during milling. Based on the DEM, KANO et al [20], MORI et al [16], and MIO et al [12,13] found that P_W can be calculated using Eq. (6). In this equation, v_j is the relative velocity corresponding to the collisions between two balls and/or of a ball against the mill wall. Equation (1) can be expressed as Eq. (8) on the basis of Eq. (6).

$$P_W = \frac{1}{t}\sum_{j=1}^{n}\frac{Mv_j^2}{2W} \tag{6}$$

$$M = \frac{2m_1m_2}{m_1+m_2} \tag{7}$$

$$\frac{1}{t}\sum_{j=1}^{n}\frac{Mv_j^2}{2W} = P_{W,m} + P_{W,n} \tag{8}$$

where W is the mass of the sample placed in the mill; n is the number of collisions of the balls per second in the mill; m is the mass of a small ball; M is the reduced mass of balls with diameter of 10 mm and 20 mm; t is the grinding time.

In this experiment, M and W were assumed to be constant. The values of P_W and n were affected only by v_j. V_s increases with $P_{W,m}$ in Eq. (8). Cascading-type motion does not occur when v is very small, owing to the centrifugal force caused by the rotation of the pot being small. In this case, v_j and P_W are very small, and hence, the value of V_s is also very small. Cascading-type motion does occur when v reaches a critical value, as can be seen from Eq. (8), owing to there being equilibrium between the centrifugal forces acting on the balls because of the rotation of the pot and the revolution of the disk. The motion changes from the cascading type to the cataracting type as v increases further. V_s peaks at 39.5 mL, indicating that most of the P_W is absorbed by the NiO/Fe_2O_3 powder and that the particle size is smaller when cascading-type motion occurs and eventually changes into cataracting-type motion. Eventually, the motion shifts from the cataracting type into the rolling type when v increases beyond the critical value. As mentioned previously, rolling-type motion is ineffective for grinding, as it results in a lower number of collisions of the individual balls and leads to collisions against the mill wall. The value of v_j decreases as the rolling speed increases, and P_W is mostly determined by $P_{W,n}$. Further, V_s also decreases with an increase in the rolling speed.

It can be seen from Fig. 4 that $P_{W,n}$ increases with an increase in v, reaching a peak value of 7.5 mJ/s. Subsequently, its value falls. Cascading-type motion does not occur when v<300.9 r/min. As both v_j and P_W are very small, so is the value of $P_{W,n}$. However, cascading-type motion takes place when $v \geq 300.9$ r/min in Eq. (8). More of P_W is absorbed by the NiO/Fe_2O_3 powder, and the particle size is smaller when cascading-type motion occurs. Hence, $P_{W,n}$ increases slightly. Then, the motion shifts from the cataracting type to the rolling type when $v \gg 300.9$ r/min. The value of v_j decreases as the extent of rolling increases, and P_W is determined mostly by $P_{W,n}$. Hence, the value of $P_{W,n}$ is extremely large. It is interesting to note that the value of V_s peaks at 39.5 mL when $P_{W,n}$ reaches a low point, and V_s reaches the lowest value when $P_{W,n}$ reaches its peak, which is 7.5 mJ/s. The above-described phenomena suggest that the grinding efficiency increases with a decrease in the degree of noisy-power dissipation.

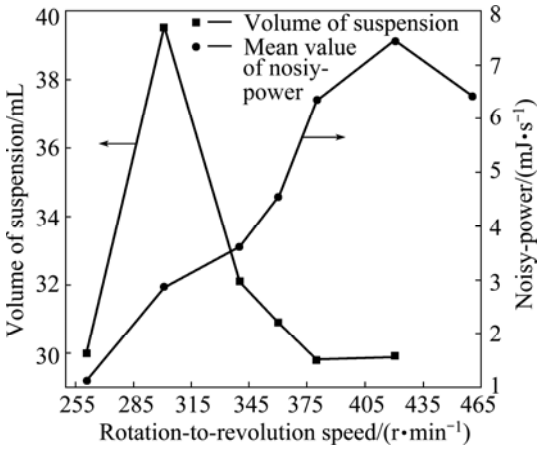

Fig. 4 Relationship among rotation-to-revolution speed, V_s, and $P_{W,s}$

3.4 Analysis of V_s and $P_{W,n}$ for different powder-filling ratios

Figure 5 reveals that both V_s and $P_{W,n}$ decrease with an increase in the powder-filling ratio when the other parameters listed in Table 3 remain unchanged. This phenomenon can be explained by Eqs. (6) and (8). With an increase in the powder-filling ratio (i.e., with an increase in W in Eqs. (6) and (8)), the powders completely cover the container walls and the milling balls. This leads to a decrease in the collision frequency (n) and v_j. Thus, P_W and $P_{W,n}$ decrease in Eqs. (6) and (8). Cascading-type motion does not occur as the powder-filling ratio is increased. On the other hand, it does occur when the powder-filling ratio is decreased. Figure 5 shows that the volume of the suspension is the highest when the powder-filling ratio is 5.44%; however, it is suggested that the powder-filling ratio is set to be ~10.88% in order to reduce the friction and wear.

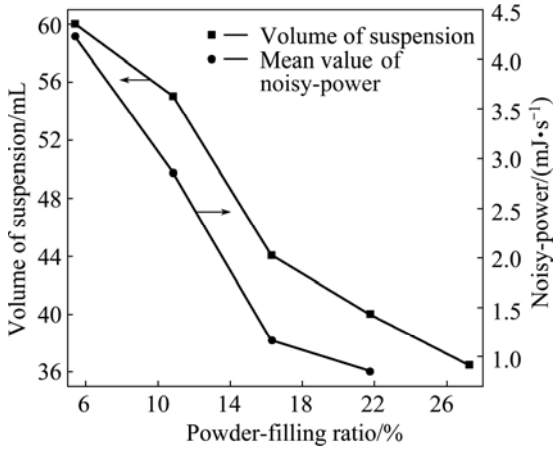

Fig. 5 Relationship among powder-filling ratio, V_s, and $P_{W,n}$

Figure 6 shows the volume of the suspension for different number ratios of the balls with diameters of 10 and 20 mm; the power-filling ratio remains the same. The number ratios are 5 and 18, respectively, for curves 1 and 2 in Fig. 6. Figure 6 also shows that V_s increases with an increase in the number ratio and that V_s decreases with an increase in the powder-filling ratio. When the powder-filling ratio is increased (i.e., W in Eqs. (6) and (8) is increased), the powder completely covers the container walls and the balls, leading to a lower collision frequency (n) and v_j. As a result, P_W in Eqs. (6) and (8) decreases. Figure 6 also suggests that V_s increases with an increase in the number ratio. Both n and v_j increase

with an increase in the ball number ratio in Eqs. (6) and (8). This causes $P_{W,m}$ to increase. Further, V_s increases with the increase in $P_{W,m}$. Finally, Fig. 5 also shows that the volume of the suspension is the maximum when the powder-filling ratio is 5.44%; however, as noted previously, it is suggested that the powder-filling ratio is set to be ~10.88% in order to reduce the friction and wear.

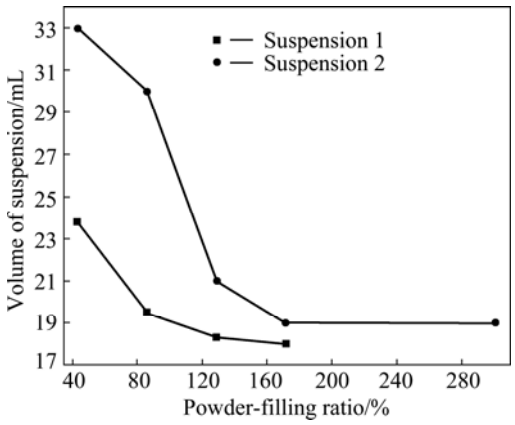

Fig. 6 Relationship between powder-filling ratio and V_s

3.5 Analysis of V_s and $P_{W,n}$ for different ball-filling ratios

Figure 7 shows the plots of the experimental values of V_s and $P_{W,n}$ as functions of the ball-filling ratio while the other parameters listed in Table 3 were kept constant. It can be seen from the figure that V_s reaches a maximum value of 44 mL when the ball-filling ratio is 20.53%−23.88%, at which $P_{W,n}$ is 0.4−0.7 mJ/s. Subsequently, the value of V_s decreases. The value of $P_{W,n}$ increases slowly when the ball-filling ratio is smaller than 20.53%. However, it increases significantly when the ball-filling ratio is greater than 23.88%.

This phenomenon can be explained by Eqs. (5), (6), and (8). It was assumed that W remained constant in this experiment. Initially, the excess NiO/Fe_2O_3 slurry that covered the container walls and the milling balls leads to

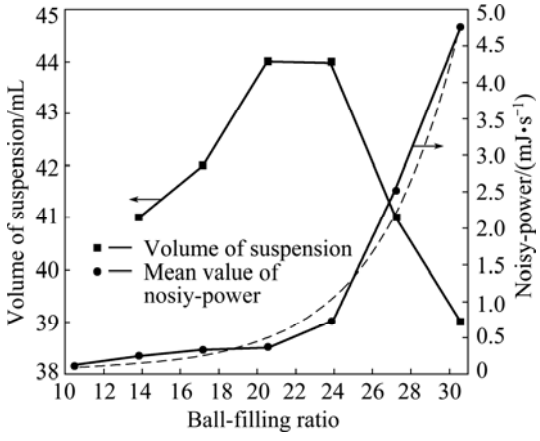

Fig. 7 Relationship among ball-filling ratio, V_s, and $P_{W,n}$

lowering of the collision frequency (n) and v_j in Eqs. (6) and (8). The μ in Eq. (5) is also very large, while v is very small, owing to the centrifugal force being small. Hence, V_s increases with an increase in the ball-filling ratio. Further, $P_{W,n}$ increases slowly with an increase in V_s. Therefore, the collision frequency (n) and v_j in Eqs. (6) and (8) increase with an increase in the ball-filling ratio (i.e., M increases in Eqs. (6) and (8)), because the extent to which the NiO/Fe_2O_3 slurry covers the container walls and the balls decreases. As result, μ, R, and ω also decrease in Eq. (5). Cascading-type motion occurs and shifts to the cataracting type with an increase in the ball-filling ratio when the term on the left-hand side in Eq. (5) is smaller than the term on the right-hand size. Thus, the value of $P_{W,m}$ increases in Eqs. (6) and (8), and V_s increases with an increase in $P_{W,m}$. However, cascading-type motion does not occur when the ball-filling ratio is increased further. This is owing to the fact that the container walls and the balls are no longer covered by the NiO/Fe_2O_3 slurry and because when the number of balls is high, it leads to lowering of the collision frequency (n) and v_j in Eqs. (6) and (8), while the volume of the mill pot remains constant. The value of mg in Eq. (5) is also very large.

It can be seen from Fig. 7 that $P_{W,n}$ increases sharply when the ball-filling ratio ≥ 23.88%. The dashed line is the nonlinear fitting line that represents the relationship between $P_{W,n}$ and the ball-filling ratio, J, in Fig. 7. The relationship between $P_{W,n}$ and J can be described empirically by Eq. (9), where the values of the empirical constants, $P^0_{W,n}$, A, and K are 5.59×10^{-5}, 3.48×10^{-6} and −4.23, respectively, within the experimental range. These values were obtained using the least squares method. By analyzing the experimental results, the constants $P^0_{W,n}$, A, and K could be explained as follows: noisy-power dissipation during planetary balling mill operation without loading, per-exponential factors, ball grinding media factors which depend on the material, respectively. The R and R^2 values for Eq. (9) were 99.4% and 98.1%, respectively.

$$P_{W,n} - P^0_{W,n} = A\exp\left(\frac{-J}{K}\right) \tag{9}$$

where K is the ball grinding media factor which depends on the material.

On the basis of the above-described results, it can be surmised that the volume of the suspension increases with a decrease in the extent of noisy-power dissipation. Thus, it can be assumed that the efficiency of planetary ball milling would decrease when the extent of noisy-power dissipation exceeds a specific value, which is determined by Eq. (9). Therefore, Eq. (9) is useful for determining the efficiency of planetary ball milling.

3.6 Analysis of V_s and $P_{W,n}$ for different grinding time

Figure 8 shows that $P_{W,n,t}$, which is the product of $P_{W,n}$ and the grinding time, increases with the grinding time as the other milling parameters, listed in Table 3, remain constant. However, V_s reaches a maximum value of 30 mL and subsequently decreases with an increase in the grinding time, as shown in Fig. 8. This is because the powder grain size is large for grinding time less than 6 h, and the finer powder particles agglomerate when the grinding time is more than 6 h. Thus, the NiO/Fe_2O_3 powder should be ground for ~6 h.

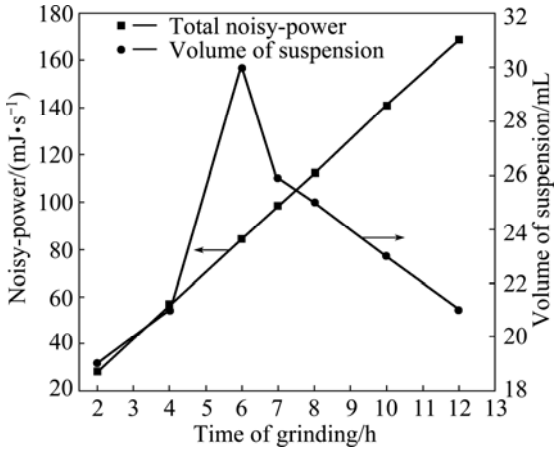

Fig. 8 Relationship among grinding time, V_s, and $P_{W,n}$

3.7 Analysis of specific surface area of ground powder

Table 4 lists the specific surface area distribution corresponding to milling conditions A to E, that is, for the optimum rotation-to-revolution speed (A), slurry water content (B), ball-filling ratio (C), powder-filling ratio (D), and grinding time (E). It can be seen from the table that the specific surface area of the NiO/Fe_2O_3 powder increases as the milling conditions are improved, resulting in a smaller mean particle size.

Table 4 Distribution of specific surface area of powder and corresponding mean particle size

Condition	Specific surface area/($m^2 \cdot g^{-1}$)	Mean particle size/μm
A	7.758	0.176
B	8.213	0.166
C	9.071	0.150
D	9.392	0.145
E	10.389	0.131

4 Conclusions

1) The effects of various grinding parameters on the characteristics of a NiO/Fe_2O_3 powder were studied using a planetary ball mill. The relationship between the noisy-power dissipation and the grinding parameters was also investigated. The DEM was employed to explain the obtained results. It was found that the optimum grinding parameters were as follows: a slurry water content of 64.1%−85.47%; a number ratio of balls with diameters of 10 and 20 mm of 360/20; a rotation-to-revolution speed ratio of 300.9 r/min; a powder-filling ratio of approximately 10.88%; a ball-filling ratio of 20.53%−23.88%; and a grinding time of approximately 6 h.

2) It was found that the mean particle size of the ground powder increased with an increase in the extent of noisy-power dissipation owing to collisions, while the milling efficiency and the degree of utilization of the specific impact energy decreased. The relationship between the extent of noisy-power dissipation and the ball-filling ratio was determined using the nonlinear fitting method.

3) The findings of this study should help to improve the efficiency of ball mill grinding of various materials.

Acknowledgements

This work was supported by the Inert Anode Material Production and Application in Electrolytic Production of Aluminium program of the Yunnan Aluminium Yonxin Aluminium Co. Ltd.

References

[1] KENIRY J. The economics of inert anodes and wettable cathodes for aluminum reduction cells [J]. JOM, 2001, 53(5): 37−43.

[2] de NORA V. Aluminium electrowinning—The future [J]. Aluminium, 2000, 76(12): 998−999.

[3] KVANDEK H. Inert electrodes in aluminium electrolysis cells [C]// ECKERT C E. Light Metals. California: TMS, 1999: 369−376.

[4] HRYN J N, SADOWAY D R. Cell testing of metal anodes for the aluminium electrolysis [C]//DAS S K. Light Metals. Colorado: TMS, 1993: 475−483.

[5] YANG Jian-hong, LIU Ye-xiang, WANG Hua-zhang. The behaviour and improvement of SnO_2-based inert anodes in aluminium electrolysis [C]//DASSK. Light Metals. Colorado: TMS, 1993: 493−495.

[6] OLSEN E, NICKEL J. Nickel ferrite as inert anodes in aluminium electrolysis: Part I. Material fabrication and preliminary testing [J]. Journal of Applied Electrochemistry, 1999, 29: 293−299.

[7] LAI Yan-qing, HUANG Li-feng, TIAN Zhong-liang, WANG Jia-wei, ZHANG Gang, ZHANG Yong. Effect of CaO doping on corrosion resistance of Cu/($NiFe_2O_4$−10NiO) cermet inert anode for aluminum electrolysis [J]. Journal of Central South University of Technology, 2008, 15(6): 743−747.

[8] DU Jin-jing , LIU Yi-han, YAO Guang-chun, ZHANG Zhi-gang. Effect of MnO_2 addition on sintering properties of 18NiO−$NiFe_2O_4$ composite ceramics: Preliminary results [J]. Journal of Materials Engineering and Performance, 2012, 21(9): 1998−2001.

[9] LAI Yan-qing, TIAN Zhong-liang, QIN Qing-wei, ZHANG Gang, LI Jie. Solubility of complex oxide ceramic in Na_3AlF_6−Al_2O_3 melt [J]. Journal of Central South University: Nature Science, 2003, 34(3): 245−248. (in Chinese)

[10] ROSENKRANZ S, BREITUNG-FAES S, KWADE A. Experimental investigations and modelling of the ball motion in planetary ball mills [J]. Powder Technology, 2011, 212(1): 224−230.

[11] LAI Yan-qing, LI Jie, TIAN Zhong-liang, ZHANG Gang, LIU Ye-xiang. An improved pyroconductivity test of spinel-containing cermet inert anodes in aluminum electrolysis cells [C]//Light Metals. Charlotte, North Carolina: TMS (The Minerals, Metals & Materials Society), 2004: 339−344.
[12] MIO H, KANO J, SAITO F, KANEKO K. Optimum revolution and rotational directions and their speeds in planetary ball milling [J]. International Journal of Mineral Processing, 2004, 74: S85−S92.
[13] MIO H, KANO J, SAITO F. Scale-up method of planetary ball mill [J]. Chemical Engineering Science, 2004, 59(24): 5909−5916.
[14] ASHRAFIAFIZADEH H, ASHRAFIAFIZADEH M. Influence of processing parameters on grinding mechanism in planetary mill by employing discrete element method [J]. Advanced Powder Technology, 2012, 23(6): 708−716.
[15] SATO A, KANO J, SAITO F. Analysis of abrasion mechanism of grinding media in a planetary mill with DEM simulation [J]. Advanced Powder Technology, 2010, 21(2): 212−216.
[16] MORI H, MIO H, KANO J, SAITO F. Ball mill simulation in wet grinding using a tumbling mill and its correlation to grinding rate [J]. Powder Technology, 2004, 143−144: 230−239.
[17] ODA M, IWASHITA K. Study on couple stress and shear band development in granular media based on numerical simulation analyses original research article [J]. International Journal of Engineering Science, 2000, 38: 1713−1740.
[18] CHOI W S, CHUNG H Y, YOON B R, KIM S S. Applications of grinding kinetics analysis to fine grinding characteristics of some inorganic materials using a composite grinding media by planetary ball mill [J]. Powder Technology, 2001, 115: 209−214.
[19] JIANG M J, YU H S, HARRIS D. A novel discrete model for granular material incorporating rolling resistance [J]. Computers and Geotechnics, 2005, 32(5): 340−357.
[20] KANO J, MIYAZAKI M, SAITO F. Ball mill simulation and powder characteristics of ground talc in various types of mill [J]. Advanced Powder Technology, 2000, 11(3): 333−342.
[21] IWASHITA K, ODA M. Micro-deformation mechanism of shear banding process based on modified distinct element method [J]. Powder Technology, 2000, 109: 192−205.
[22] GUDIN D, KANO J, SAITO F. Effect of the friction coefficient in the discrete element method simulation on media motion in a wet bead mill [J]. Advanced Powder Technology, 2007, 18(5) : 555−565.

NiO/Fe_2O_3 湿式行星球磨中的噪声能消耗与效率

姚 云[1]，谢 刚[1,2]，侯彦青[1]，李荣兴[1]，罗伟红[1]，彭如振[1]，于站良[2]

1. 昆明理工大学 冶金与能源学院，昆明 650093；2. 昆明冶金研究院，昆明 650031

摘 要：研究 NiO/Fe_2O_3 湿式混合与球磨过程中的噪声能消耗、球磨效率及二者之间的关系。结果表明，球磨工艺的最佳工艺参数为：填水率 64.10%~85.47%，小/大球个数比 360/20，球磨机转速 300.9 r/min，填粉率约 10.88%，填球率 20.53%~23.88%，球磨时间 6 h。引入离散元法(DEM)分析球磨过程中噪声能消耗与球磨效率之间的关系，得到噪声能消耗与填球率关系的经验方程。研究表明粉体的平均粒度随着噪声能的消耗而减小，而球磨效率和球碰撞能的利用率则随着噪声能消耗的增加而减小。

关键词：噪声能消耗；NiO/Fe_2O_3 粉体；行星式球磨；平均粒度

(Edited by Xiang-qun LI)